Selected references
1 **Cooper, J.R., Bloom, F.E. and Roth, R.H.** (1996) *The Biochemical Basis of Neuropharmacology*, Oxford University Press
2 **Clements, J.D.** (1996) *Trends Neurosci.* 19, 163–171
3 **Fuxe, K. and Agnati, L.F., eds** (1991) *Volume Transmission in the Brain: Novel Mechanisms for Neural Transmission*, Raven Press
4 **Garris, P.A. and Wightman, R.M.** (1994) *J. Neurosci.* 14, 442–450
5 **Travis, E.T. and Wightman, R.M.** (1998) *Annu. Rev. Biophys. Biomol. Struct.* 27, 77–103
6 **Stamford, J.A. and Justice, J.B.** (1996) *Anal. Chem.* 68, 359A–368A
7 **Garris, P.A. *et al.*** (1994) *J. Neurosci.* 14, 6084–6093
8 **Bunin, M.A. and Wightman, R.M.** (1998) *J. Neurosci.* 18, 4854–4860
9 **Trussell, L.O. and Fischbach, G.D.** (1989) *Neuron* 3, 209–218
10 **Edgar, P.P. and Schwartz, R.D.** (1991) *Mol. Pharmacol.* 41, 1124–1129
11 **Triller, A. and Korn, H.** (1982) *J. Neurophysiol.* 48, 708–736
12 **Neale, E.A. *et al.*** (1983) *J. Neurophysiol.* 49, 1459–1468
13 **Clements, J.D. *et al.*** (1992) *Science* 258, 1498–1501
14 **Schonrock, B. and Bormann, J.** (1993) *Eur. J. Neurosci.* 5, 1042–1049
15 **Tang, C-M. *et al.*** (1994) *Neuron* 13, 1385–1393
16 **Perrais, D. and Ropert, N.** (1999) *J. Neurosci.* 19, 578–588
17 **Barbour, B. *et al.*** (1994) *Neuron* 12, 1331–1343
18 **Lehre, K. and Danbolt, N.C.** (1998) *J. Neurosci.* 18, 8751–8757
19 **Thompson, S.M. and Gahwiler, B.H.** (1992) *J. Neurophysiol.* 67, 1698–1701
20 **Sarantis, M. *et al.*** (1993) *Neuron* 11, 541–549
21 **Kullmann, D.M., Erdmli, G. and Asztely, F.** (1996) *Neuron* 17, 461–474
22 **Isaacson, J.S., Solis, J.M. and Nicoll, R.A.** (1993) *Neuron* 10, 165–175
23 **Asztely, F., Erdemli, G. and Kullmann, D.M.** (1997) *Neuron* 18, 281–293
24 **Baude, A. *et al.*** (1993) *Neuron* 11, 771–787
25 **Somogyi, P. *et al.*** (1989) *J. Neurosci.* 9, 2197–2209
26 **Spreafico, R. *et al.*** (1993) *Neurosci. Lett.* 158, 232–236
27 **Chazal, G. and Ralston, H.J., III** (1981) *J. Comp. Neurol.* 259, 317–329
28 **Moukhles, H. *et al.*** (1997) *Neuroscience* 76, 1159–1171
29 **Pazos, A. and Palacios, M.** (1985) *Brain Res.* 346, 205–230
30 **Kia, H.K. *et al.*** (1996) *J. Neurosci. Res.* 46, 697–708
31 **Zhou, F.C. *et al.*** (1998) *Brain Res.* 805, 241–254
32 **Chen, H.T., Clark, M. and Goldman, D.** (1992) *J. Pharmacol. Toxicol. Meth.* 27, 209–216
33 **Green, J.P. and Maayani, S.** (1987) *Perspectives on Receptor Classification* (Black, J.W., Jenkinson, D.H. and Gerskowitch, V.P., eds), Alan R. Liss
34 **O'Conner, J.J. and Kruk, Z.L.** (1992) *Br. J. Pharmacol.* 106, 524–532
35 **Bunin, M.A. *et al.*** (1998) *J. Neurochem.* 70, 1077–1087
36 **Kawagoe, K.T. *et al.*** (1992) *Neuroscience* 51, 55–64
37 **Garris, P.A. and Wightman, R.M.** (1995) *Neuromethods: Voltammetric Methods in Brain Systems* (Vol. 27) (Boulton, A.A., Baker, G.B. and Adams, R.N., eds), Humana Press
38 **Limberger, N. *et al.*** (1991) *Arch. Pharmacol.* 344, 623–629
39 **Bruns, D. and Jahn, R.** (1995) *Nature* 377, 62–65
40 **Korn, H. *et al.*** (1982) *J. Neurophysiol.* 48, 679–707
41 **Neale, E.A. *et al.*** (1983) *J. Neurophysiol.* 49, 1459–1468
42 **Silver, R.A., Momiyama, A. and Cullcandy, S.G.** (1998) *J. Physiol.* 510, 881–902
43 **Canepari, M. and Cherubini, E.** (1998) *J. Neurophysiol.* 79, 1977–1988
44 **Wang, R.Y. and Aghajanian, G.K.** (1982) *J. Neurosci.* 2, 11–16
45 **Pickel, V.M. *et al.*** (1981) *Brain Res.* 225, 373–385
46 **Giros, B. *et al.*** (1996) *Nature* 379, 606–612
47 **Rothstein, J.D. *et al.*** (1996) *Neuron* 16, 675–686
48 **Chaudhry, F.A. *et al.*** (1995) *Neuron* 15, 711–720
49 **Ribak, C.E., Tong, W.M. and Brecha, N.C.** (1996) *Anat. Embryol.* 194, 379–390
50 **Minelli, A. *et al.*** (1996) *J. Neurosci.* 16, 6255–6264

Acknowledgement
The authors' research was supported by the National Institute of Health (NS 15841).

Hippocampal synapses: do they talk to their neighbours?

Dmitri A. Rusakov, Dimitri M. Kullmann and Michael G. Stewart

Recent experimental findings show that fast synaptic transmission can extend its actions beyond the immediate synaptic cleft. Whether this phenomenon results in significant crosstalk between typical neighbouring synapses remains unclear. This article considers two areas of the hippocampus, the CA1 and dentate gyrus, where important neural processing occurs. The results discussed do not provide a simple answer to the question of whether synapses can 'talk' to their neighbours, but they do reveal crucial physiological constraints that determine the significance of synaptic crosstalk, thus adding considerably to our understanding of chemical synaptic transmission.

Trends Neurosci. (1999) 22, 382–388

Dmitri A. Rusakov is at the Division of Neurophysiology, National Institute for Medical Research, London, UK NW7 1AA, Dimitri M. Kullmann is at the University Dept of Clinical Neurology, Institute of Neurology, University College London, London, UK WC1N 3BG, and Michael G. Stewart is at the Dept of Biology, The Open University, Milton Keynes, UK MK7 6AA.

MUCH EVIDENCE has emerged recently to suggest that basal transmission at conventional 'fast' CNS synapses exerts actions that extend beyond the synaptic cleft. On the one hand, synaptically released GABA and glutamate appear to bind to receptors that are at a considerable distance from the activated synapse[1–4]. On the other hand, synaptic activity might cause transient depletion of extracellular Ca^{2+} in the synaptic vicinity and thus affect synaptic communication[5,6]. This article aims to examine recent evidence concerning the spatial separation of synapses in the hippocampus and to consider the consequences for possible interactions between neighbouring synapses.

Some of the experimental observations and theoretical implications regarding extrasynaptic neurotransmitter spillover have recently been discussed[7,8]. An alternative insight into the extracellular neurotransmitter concentration profiles that follow exocytosis comes from an examination of the currents elicited in astrocytes by electrogenic glutamate uptake. Transporter currents in hippocampal slices are considerably slower than those observed in outside–out membrane patches of astrocytes following rapid application of glutamate[9]. This observation implies that an elevated glutamate concentration persists for a long time (possibly as long as 10 milliseconds) in the vicinity of glial transporters, which could be a considerable distance from the release site[10].

Relatively little is known about the kinetics of local Ca^{2+} depletion. At a calyceal central synapse, approximately 2.5×10^6 Ca^{2+} ions have been estimated to flow into the presynaptic terminal during an action potential[11]. If Ca^{2+} enters the cell exclusively from the synaptic

  PII: S0166-2236(99)01425-3

Box 1. Distances between nearest neighbours in a synaptic scatter

The mean nearest-neighbour distance (NND), r_0, between synapses in the neuropil is determined not only by the numerical volume density of synapses, N_V, but also by their spatial arrangement. This is illustrated in Fig. IA–C where three characteristic point patterns are shown. These patterns exhibit the same numerical density (N_V) but different distributions of NNDs and consequently different values of r_0. In the case of a regular square lattice (Fig. IA) in 3D, geometry gives $r_0 = N_V^{-1/3}$, whereas a uniformly random or Poisson scatter (Fig. IB) in 3D gives $r_0 \sim 0.554\ N_V^{-1/3}$ (Ref. a). However, the synaptic centroids (which we define here as the geometric centres of the synaptic clefts) cannot be closer to each other than is allowed by the 3D sizes of the synapses. A common stereological measure of the synaptic size is the mean projected height of the synapses, which in fact represents the mean 'calliper' diameter (in 3D) of synaptic elements that are immediately associated with the synaptic cleft[a]. Setting the mean size of synapses, d (illustrated as shadowed circular areas in Fig. IC) results in an additional correction for r_0, which can be estimated using a Monte-Carlo experiment as follows. First, a Poisson point process (uniformly random scatter) is generated with a numerical density that is slightly higher than N_V. Second, points located at distances that are smaller than d from their nearest neighbours are deleted. Third, the numerical density of the remaining points (N_V*) is calculated. Fourth, the entire procedure is repeated with a higher initial density until $N_V^* = N_V$. This algorithm is also known as the Matern process of rigid spheres[b] because it is equivalent to throwing a known number of weightless solid spheres into a box of known dimensions. This methodology was adopted in our previous work to study populations of dendritic spines[c,d]. By avoiding points located near the box edges (these will give biased measurements and must not be sampled[b]), the NND is found for each point within the generated scatter.

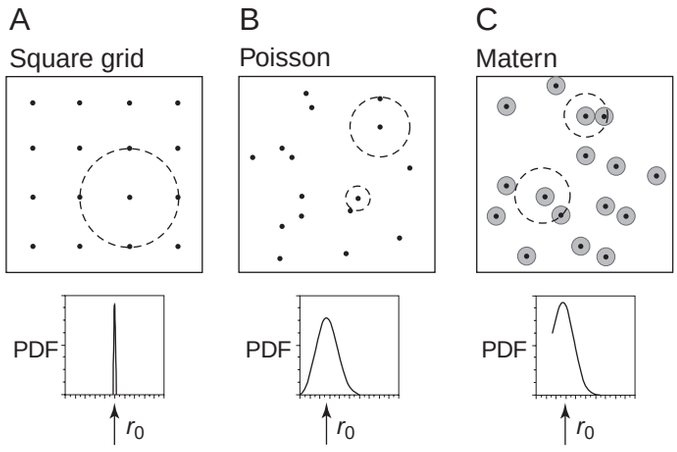

Fig. I. ***Nearest neighbour distances (NNDs) for different point patterns.*** *Three different point patterns are shown: points arranged at square-grid vertices* **(A)***; a uniformly random pattern or Poisson process* **(B)***; and a uniformly random pattern with the size constraint (shown by shadowed circles), which is termed a hard-core Poisson or Matern process of rigid spheres* **(C)**. *The corresponding distributions (probability density functions, PDF) of NNDs are illustrated in the lower panels. The broken line circles (upper panels) indicate NNDs for several points and the arrows (lower panels) indicate the mean NND,* r_0.

References

a Brændgaar, H. and Gundersen, H.J.G. (1986) *J. Neurosci. Methods* 18, 39–78

b Stoyan, D., Kendall, W.S. and Mecke, J. (1987) *Stochastic Geometry and Its Applications*, John Wiley & Sons

c Rusakov, D.A. *et al.* (1995) *NeuroReport* 6, 1557–1561

d Rusakov, D.A. *et al.* (1997) *Hippocampus* 7, 489–500

cleft, this implies that there will be a profound local depletion of this ion: assuming a cleft width of 20 nm and a synaptic apposition area of 100 μm^2, the Ca^{2+} concentration in the cleft would drop by ~2 mM. Even if this Ca^{2+} influx is less localized, the increase in presynaptic Ca^{2+} concentration of 10–13 μM in these synapses[12] suggests a more widespread drop of extracellular Ca^{2+} concentration, by ~0.1 mM, as the extracellular space occupies 12–15% of the tissue volume[13]. This estimation, however, ignores Ca^{2+} diffusion into the cleft and the adjacent medium from the neighbouring extracellular space, which presumably has a major role in supplying Ca^{2+} during repetitive synaptic activity[14]. Conversely, it also ignores postsynaptic Ca^{2+} influx, which acts as a further sink for extracellular Ca^{2+}. A fundamental consequence of these phenomena is a reduction in the extracellular Ca^{2+} concentration, a signal that could propagate rapidly through the neighbouring tissue[5].

If significant glutamate spillover and transient Ca^{2+} depletion exist in the vicinity of the synapse, does this affect neighbouring synapses? The answer to this question depends on the spatial arrangement of synapses, which varies extensively between different pathways in the brain. For example, cerebellar glomeruli contain mossy-fibre nerve terminals, as well as Golgi-cell boutons and granule-cell processes, enclosed within a glial envelope within which $GABA_A$ receptors appear to detect both direct and remote (spillover) neurotransmitter release[15,16]. The question raised here is whether synaptic crosstalk occurs at more typical central synapses, for example, at excitatory synapses on pyramidal neurones in the CA1 region of the hippocampus. These synapses are among the most thoroughly characterized, not least because they exhibit NMDA-receptor-dependent LTP. If synapses are generally able to influence their neighbourhood, either by transmitter spillover or by Ca^{2+} depletion, a radical alteration will be required in our understanding of intercellular signalling in the brain.

Clearly, one crucial parameter that affects synaptic crosstalk is the typical distance separating one synapse from its nearest neighbour (the 'nearest-neighbour distance' or NND). Estimating this parameter is not a trivial task. We recently approached this problem by combining Monte-Carlo simulations with unbiased stereological measures from electron micrographs of the hippocampal neuropil. This article analyses these estimates and compares them with novel data obtained from 3D reconstruction of serial sections. Combined with numerical simulations of diffusion fluxes in the synaptic vicinity, these data provide a novel insight into the plausibility of synaptic crosstalk caused by glutamate spillover and transient Ca^{2+} depletion.

Distances between synapses: statistical estimation from representative samples

The mean NND is related to the number of synapses per unit tissue volume. However, given the same numerical density, distinct 3D arrangements of synapses can give very different values for the mean NND. This principle is illustrated in Box 1, where the mean NNDs are compared for three characteristic examples: synapses arranged in a regular lattice, scattered randomly or scattered randomly with a minimum separation. In our earlier attempt to analyse the arrangement of hippocampal

Box 2. The mean nearest-neighbour distance between synapses: Monte-Carlo estimates and 3D reconstruction from serial sections

Given that the distribution of synapses can be reasonably approximated by a hard-core Poisson or Matern scatter, only two experimental measures are needed to determine the mean nearest-neighbour distance (NND): the mean synaptic density, N_V, and the mean size of synapses, *d*. Alternatively, a small sample of direct measurements of NNDs can be obtained using 3D reconstruction of a tissue fragment from serial sections. In our experiments, 14 ultra-thin (60–75 nm, estimated according to Ref. a) serial sections were taken from area CA1 in the rat hippocampus. (In larger samples of serial sections, it was difficult to control the accumulated alignment bias that is typical for the large sampling windows we used.) The sections were collected on Pioloform-coated grids and analysed using an electron microscope[b,c]. Fields of interest in the neuropil (14 μm wide, 10 μm high) were imaged and aligned in consecutive sections. In each individual section, the 2D coordinates of the centres of all postsynaptic densities (PSDs) were recorded. From these data, the 3D position of each intact PSD was computed as the centroid of all serial fragments that represented the same PSD (similar to reconstruction routines in Ref. d). Within the reconstructed block of tissue, values of synaptic density (N_V =1.25 μm^{-3}) and mean synaptic size (*d* = 220 nm) were obtained. Figure IA shows a Matern scatter of spheres generated using the Monte-Carlo algorithm and the above values of *d* and N_V. Figure IB illustrates the synaptic scatter reconstructed directly from the stack of serial sections. Thus, data in Fig. I allow not only a numerical comparison but also a visual comparison of Monte-Carlo experiment results and 3D-reconstruction data within a similar slab of tissue.

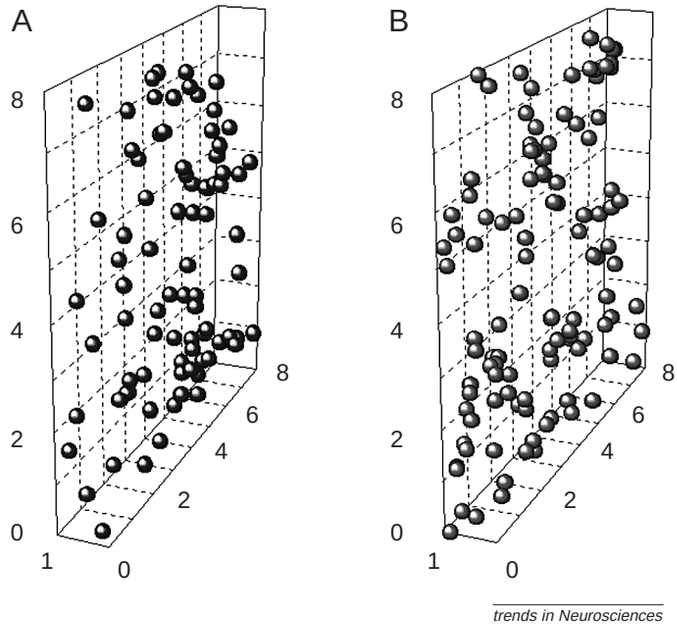

Fig. I. ***An example of a 3D-synaptic pattern obtained using a Monte-Carlo simulation experiment*** **(A)** ***and 3D reconstruction from serial sections*** **(B).** *An 8 μm × 8 μm x 1 μm fragment of synaptic scatter in neuropil is illustrated. The same values of mean synaptic size,* d *= 220 nm, and numerical density,* N_V *=1.25 μm^{-3}, apply to both diagrams [*(A) *and* (B)*], and were obtained in a block reconstructed from serial sections. The sphere diameter corresponds to* d *(Ref. e). The values of nearest-neighbour distance in these examples were found to be ~0.52 μm [*(A)*, Monte-Carlo estimate] and ~0.48 μm [*(B)*, 3D reconstruction].*

References
a DeGroot, D.M.G. (1988) *J. Microsc.* 151, 23–42
b Doubell, T.P. and Stewart, M.G. (1993) *J. Neurosci.* 13, 2230–2236
c Rusakov, D.A. *et al.* (1997) *Neuroscience* 80, 69–77
d Schikorski, T. and Stevens, C.F. (1997) *J. Neurosci.* 17, 5858–5867
e Brændgaar, H. and Gundersen, H.J.G. (1986) *J. Neurosci. Methods* 18, 39–78

synapses in area CA1 and in the dentate gyrus of the hippocampus we found no regular pattern. The minimum distance between the centres of the synaptic profiles was, however, restricted by the size of the synapses themselves[17] (this size can be thought of as twice the mean distance between the synaptic-cleft centre and the closest nonsynaptic element of the neuropil in 3D). In terms of stochastic geometry, this type of scatter is termed a hard-core Poisson process, or is sometimes described as the Matern process for rigid spheres because it is analogous to spheres scattered randomly in space. It seems reasonable to approximate the local distribution of synapses with such a pattern. In this case, the mean NND can be estimated from a Monte-Carlo sampling experiment that uses two experimental measures: the numerical synaptic density, N_V, and the mean synaptic size (or projected height[18]), *d*, as explained in Box 2. The values of N_V and *d* in area CA1 and dentate gyrus have been obtained from our previous work[17]. These estimates were consistent with earlier reports by Geinisman and colleagues[19], and also included a measured tissue-shrinkage factor for the electron-microscopy embedding protocol we used, ~6% for linear measurements and ~16% for volumetric measurements[20].

In Monte-Carlo simulations, the mean NND is estimated by generating large samples (n>1000) of synaptic coordinates scattered in a cube so that their numerical density matches N_V, as described in more detail in Box 1. Once the appropriate scatter is generated, measuring distances between nearest neighbours is straightforward. Figure 1 shows histograms of inter-synaptic distances measured in such samples and gives a mean NND of ~0.48 μm for dentate gyrus and of ~0.49 μm for area CA1 (including the correction for tissue shrinkage).

Distances between synapses: direct measurements from 3D reconstruction

Although the methods underlying the Monte-Carlo assessment are based on the use of representative samples of data (sections are sampled throughout the region of interest in several animals), it is useful to have a direct verification of the estimated mean NND. This can be achieved by using 3D reconstruction of a tissue fragment from serial ultra-thin sections, as described and illustrated in Box 2. Our 3D-reconstruction experiment yielded the NND histogram shown in Fig. 2, which gives a mean NND of 0.48 μm. Given that N_V = 1.25 μm^{-3} in this particular sample, the corresponding Monte-Carlo estimate of NND is ~0.52 μm. Box 2 provides an example of the synaptic scatter generated in our Monte-Carlo experiments and the scatter of similar dimensions obtained from serial sections via 3D reconstruction. Harris and Ventura have recently reported preliminary results of their 3D-reconstruction study in which they estimate the mean distance between neighbouring synapses in CA1 stratum radiatum as ~0.6 μm (Ref. 21). Given that their measure of NND also included an element of the extracellular space tortuosity, and that each reconstructed stack represents a relatively small

volume of tissue in one animal, the consistency between the two 3D-reconstruction measures and the Monte-Carlo estimate of NND is reasonable.

These data, therefore, indicate that the mean NND between centres of synaptic clefts in dentate gyrus or area CA1 is around 0.5 μm rather than 1.0 μm, the value often deduced from observing 2D-electron micrographs (see discussion in Ref. 20). What are the implications of this structural constraint for inter-synaptic crosstalk?

Diffusion of neurotransmitter following exocytosis

Following exocytosis, neurotransmitter diffuses rapidly within the synaptic cleft and further into the extracellular space. Does this diffusion activate synaptic receptors at the neighbouring synapse? Experimental detection of neurotransmitter levels with this temporal and spatial resolution is not yet feasible so the alternative is to try to answer a simple question: what do the laws of physics predict regarding extrasynaptic diffusion? A common criticism of any analytical approach is that we simply do not know many constraints that are built into a particular model (for example, the amount of glutamate released or the density of its binding sites). However, a simple test for robustness of the conclusions drawn from modelling is to explore the unknown parameters over the known physiological range. This approach has been applied successfully in several studies[22–24], which include Monte-Carlo simulations where movements of individual molecules of neurotransmitter have been traced explicitly[25–27]. One constraint, however, remains to be clarified in such simulations: how to represent the geometry of the synaptic micro-environment for the synaptic population of interest.

Box 3 illustrates an experimental approach that we used recently to address this issue. We analysed a statistical sample of electron micrographs of synapses in order to establish the occurrence of the perisynaptic extracellular space around synaptic profiles in area CA1 of the hippocampus[13]. We used this average occurrence profile to build a 3D model of the typical synaptic environment, where glutamate diffusion of arbitrary complexity could be simulated without resorting to analytical solutions, as explained in Box 3. Figure 3A shows simulated concentration transients for glutamate at different distances from the release site. The time course of the opening probability of AMPA- and NMDA-receptor channels that follows such transients is shown in Fig. 3B. Over the plausible range of physiological parameters, these simulations predict that NMDA (but not AMPA) receptors localized at neighbouring synapses are likely to be activated, especially if the extracellular diffusion coefficient of glutamate is lower than in a free medium. Several nonspecific phenomena, which have been identified as geometric (steric) and viscous (hydrodynamic) components of the extracellular space tortuosity, contribute to the retardation of the extracellular diffusion of glutamate and other small molecules in the brain[28]. Detailed simulations of extracellular diffusion also indicate a phenomenon, which is specific to glutamate and other neurotransmitters, that could further retard diffusion at low concentration levels: the buffering effect of high-affinity binding sites[13]. Glutamate transporters have an ambivalent role. On the one hand, they can act as buffers, slowing down diffusion, thereby enhancing the activation of receptors and explaining the prolonged persistence of glutamate in the vicinity of glial membranes as judged by the time course of transporter currents[9,29]. On the other hand, transporters can also bind a large fraction of the released glutamate rapidly, reducing the free-glutamate concentration and reducing the activation of its receptors. The steep temperature dependence of glutamate transport could explain why inter-synaptic spillover detected by NMDA receptors is greatly reduced when examined at physiological temperature rather than at room temperature[30].

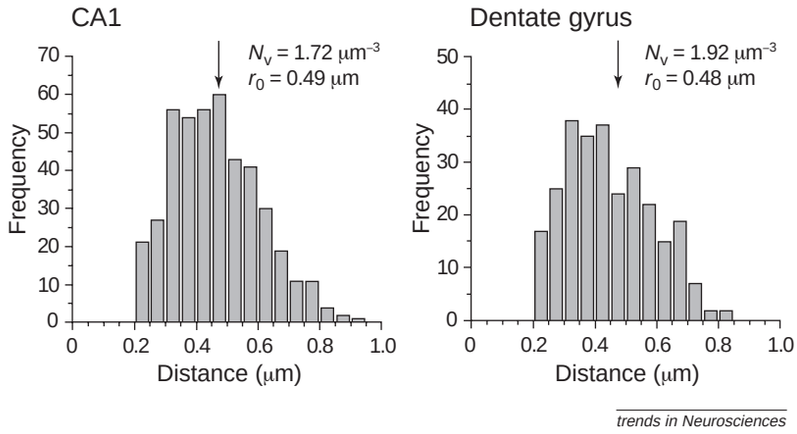

Fig. 1. ***Histograms of the nearest-neighbour distances between excitatory synapses obtained from Monte-Carlo experiments that model synaptic scatters in hippocampal neuropil.*** *The arrows indicate the mean value (also denoted as r_0). The values of numerical synapse density, N_v, account for tissue shrinkage and the mean synaptic size parameter, d, is 0.23 μm. The experimental values of N_v and d were calculated in accordance with the Disector technique using adjacent ultra-thin (~65 nm) sections taken throughout the regions of interest from four (CA1) and six (dentate gyrus) animals[13,20].*

Transients of extracellular Ca^{2+} following synaptic activation

Although synaptic activity is likely to elicit substantial Ca^{2+} depletion in the synaptic vicinity, extracellular Ca^{2+} transients have only been measured relatively indirectly, with low spatial and temporal resolution relative to inter-synaptic distances and time courses of release, respectively[31,32]. The extent to which Ca^{2+} depletion might affect neighbouring synapses remains unclear. In this study, we combined our geometric model of the synaptic environment in area CA1 with the available

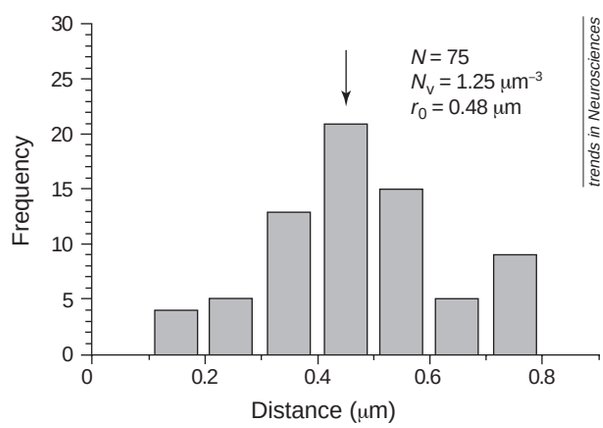

Fig. 2. ***Histogram of nearest-neighbour distances between synapses measured in a fragment of neuropil reconstructed in 3D.*** *Nearest-neighbour distances (NNDs) were measured between synaptic cleft centres in a 13 μm × 9 μm × 0.95 μm block of tissue from area CA1 of rat hippocampus, which was reconstructed in 3D using a serial section technique. The arrow indicates the mean NND (r_0), N represents the number of measured distances and N_v represents numeric synaptic density.*

Box 3. Modelling perisynaptic diffusion of neurotransmitter molecules and Ca^{2+} ions

We attempted to quantify the typical geometry of the synaptic microenvironment by analysing samples of electron micrographs: profile fragments of the extracellular space surrounding 88 axo–spinous synapses were aligned with respect to the synaptic-cleft centre and then superimposed as described by Rusakov and Kullmann[a]. The outcome of this procedure is shown in Fig. IA, where the grey level indicates the probability of encountering the extracellular space at different positions relative to the synaptic cleft (darker grey represents higher probability). These results allow one to build a realistic 3D model of the typical synaptic environment, of which a 2D cross-section is shown in Fig. IB. In this model, the neurotransmitter is released into a ~220 nm wide, 20 nm thick cleft between two hemispherical obstacles to diffusion, which represent the presynaptic and postsynaptic elements. Beyond the cleft and obstacles, the neurotransmitter moves within a homogeneous porous medium, a robust approximation that reduces the effect of geometric obstacles to two parameters: the extracellular volume fraction, α, and the geometric tortuosity, λ (Refs b,c). Morphometric analysis of neuropil in CA1 performed in our earlier study gave $\alpha = 0.12$ and $\lambda = 1.36$ (Ref. a). The value $\lambda \sim 1.4$ was subsequently confirmed to be unique for an isotropic porous medium with no preferred orientation of planar 2D pores[d].

The space in this model was divided into small compartments (thin concentric shells) to allow direct computation of the mass transfer of glutamate (or Ca^{2+}) in accordance with Fick's first law. Given sufficiently small time steps and a suitable shell width, this procedure has no limitations regarding the complexity of the reactions involved. Glutamate release from the synaptic vesicle (which contains 5000 molecules) was represented by the function $\phi(t) = t\ \sigma^2 \exp(-\sigma\ t)$ with $\sigma = 39\ ms^{-1}$ (Ref. e). The extracellular diffusion coefficient for glutamate was varied systematically between 0.2 $\mu m^2\ ms^{-1}$ and 0.75 $\mu m^2\ ms^{-1}$ in order to reflect retarded diffusion caused by geometric or viscous components of λ, or both (Ref. d). Glutamate transporters present in cell membranes had binding, unbinding and translocation rates of 5000 $M^{-1}\ ms^{-1}$, 0.1 ms^{-1} and 0.02 ms^{-1}, respectively[f,g]. The activation of AMPA and NMDA receptors at different distances from the release site was computed in accordance with kinetic schemes proposed by Lester and Jahr[h] and Jonas *et al.*[i], respectively.

The same geometric model was used to compute extracellular Ca^{2+} transport following synaptic activation. The presynaptic Ca^{2+} influx that triggers exocytosis has been studied with sufficient accuracy to justify the modelled parameters[j–l]. In this case, synaptic activation (through action potential) opened $n = 10$ presynaptic voltage-gated channels with an α-function opening time course: $Q(t) = nQ_0\sigma^2 t \exp(-\sigma^2 t)$, where $Q_0 = I/(ZeN_A)$, $I = 0.5$ pA (an individual peak channel current), $Z = 2$ for Ca^{2+}, $e = 1.9 \times 10^{-19}$ C is the elementary charge, $N_A = 6 \times 10^{23}\ mol^{-1}$ (Avogadro's number), and $\sigma = 20\ ms^{-1}$ (Refs j,m,n). During Ca^{2+} depletion, this influx current was attenuated with a proportionality factor of *ln* (extracellular Ca^{2+} concentration ÷ intracellular Ca^{2+} concentration), in accordance with the Nernst equation. Active Ca^{2+} extrusion was represented by a first-order process[o], with a rate of ~0.5 ms^{-1} (Ref. m), which also incorporates an estimate of the cell-membrane surface area per unit volume[p]. Less is known about postsynaptic Ca^{2+} influx through various channels. However, it is reasonable to assume that its time course in sub-threshold conditions is dictated mainly by the NMDA-receptor-mediated depolarization, which we have represented as a difference between two exponentials, according to Zador and Koch[o]: $I(t) = I_0\{\exp(-t/\tau_1) - \exp(t/\tau_2)\}$, where I_0 reflects the peak current, $\tau_1 = 80$ ms and $\tau_2 = 3$ ms. Postsynaptic Ca^{2+} influx was restricted to the dendritic spine (represented by postsynaptic membranes extending 0.25 μm from the synaptic cleft centre). The crucial unknown parameter explored in these simulations was the total peak Ca^{2+}-current density through channels in the postsynaptic membrane.

This model does not consider the role of Ca^{2+} ions that accumulate near cell membranes to form part of the electrical charge-screening layer, which apparently includes two components. The first component arises from the surface excess charge density, σ, induced by the depolarized membrane. The value of σ can be assessed from a simple formula for the planar capacitor: $\sigma = \epsilon\epsilon_0 V_m s^{-1}$, where ϵ is the membrane dielectric constant (~2), ϵ_0 is the permittivity of vacuum, s is the membrane thickness (~5 nm), and V_m is the membrane potential (70 mV). This formula gives $\sigma \sim 2.5 \times 10^{-4}\ C/m^2$ implying an excess density of divalent ions of $\sim 10^3\ \mu m^{-2}$. Given an intercellular gap width of ~20 nm, this corresponds to V_m-dependent changes of local extracellular Ca^{2+} concentration at a level of less than ~0.1 mM, which is unlikely to affect our calculations. The second component is due to acidic phospholipids of cell membranes, which induce an electrostatic potential (ϕ) that ranges from −10 to −100 mV in the extracellular space (Ref. q). This predicts a 100- to 1000-fold increase in Ca^{2+} levels near the membrane surface, according to the classical Debye–Hückel theory (or its Gouy–Chapman modification). However, it remains to be ascertained whether the classical theory is readily applicable in this case: for example, sub-membrane ion densities that exceed ~0.25 nm^{-2} would be inconsistent with Debye's radius of ~1 nm, which is characteristic for the extracellular medium. Furthermore, the thermal energy of sub-membrane Ca^{2+} ions, kT (where k is the Boltzmann constant and T is temperature), and their electric energy, $ze\phi$ (where $z = 2$, and e is the elementary charge), appear to be of the same order of magnitude (~10^{-21} J), in which case the ion distribution might not follow the classical theory. Finally, it is unlikely that any release of these Ca^{2+} ions 'bound' by the fixed ϕ potential is as rapid as Ca^{2+} diffusion in the free extracellular medium. The issue of the sub-membrane Ca^{2+} store, however, requires more experimental tests and detailed theoretical consideration.

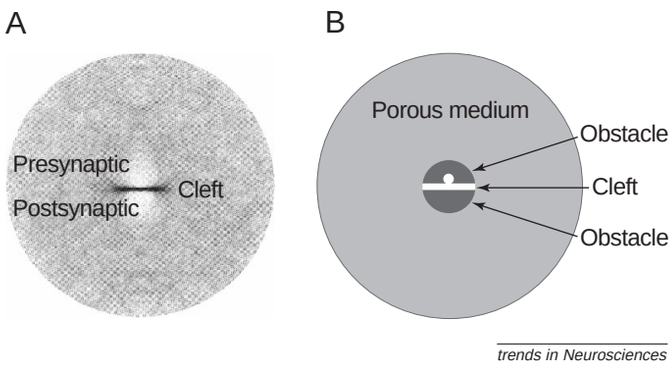

Fig. I. ***Geometry of the typical synaptic environment.*** **(A)** *Semi-transparent superimposition of the binary traces of extracellular space profiles in the vicinity of 88 excitatory synapses in CA1 area. Profiles taken from each electron micrograph were rotated and aligned with respect to the common origin, the centre of the synaptic cleft.* **(B)** *shows a 2D section of a 3D-geometric model that corresponds to the typical synaptic environment shown in* (A).

References

a Rusakov, D.A. and Kullmann, D.M. (1998) *J. Neurosci.* 18, 3158–3170
b Nicholson, C. (1985) *Brain Res.* 333, 325–329
c Nicholson, C. and Syková, E. (1998) *Trends Neurosci.* 21, 207–215
d Rusakov, D.A. and Kullmann, D.M. (1998) *Proc. Natl. Acad. Sci. U. S. A.* 95, 8975–8980
e Stiles, J.R. *et al.* (1996) *J. Neurosci.* 18, 3158–3170
f Lehre, K.P. and Danbolt, N.C. (1998) *J. Neurosci.* 18, 8751–8757
g Wadiche, J.I. *et al.* (1995) *Neuron* 14, 1019–1027
h Lester, R.A. and Jahr, C.E. (1992) *J. Neurosci.* 12, 635–643
i Jonas, P., Major, G. and Sakmann, B. (1993) *J. Physiol.* 472, 615–663
j Zucker, R.S. *et al.* (1991) *Ann. New York Acad. Sci.* 635, 191–207
k Borst, J.G.G. and Sakmann, B. (1996) *Nature* 383, 431–434
l Regehr, W. (1997) *Biophys. J.* 73, 2476–2488
m Helmchen, F., Borst, J.G.G. and Sakmann, B. (1997) *Biophys. J.* 72, 1458–1471
n Sabatini, B.L. and Regehr, W.G. (1998) *Biophys. J.* 74, 1549–1563
o Zador, A. and Koch, C. (1994) *J. Neurosci.* 14, 4705–4715
p Rusakov, D.A., Harrison, E. and Stewart, M.G. (1996) *Neuropharmacology* 75, 315–323
q Peitzsch, R.M. *et al.* **(1995)** *Biophys. J.* 68, 729–738

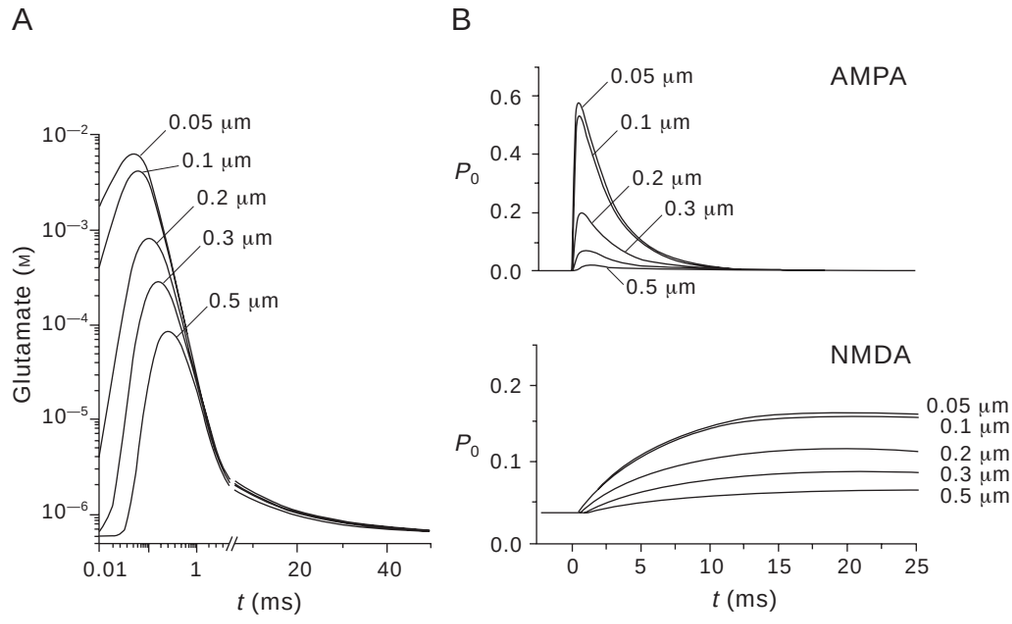

Fig. 3. ***Computed glutamate transients and activation of AMPA and NMDA receptors in the vicinity of an axospinous synapse.*** *The geometrical representation of the synaptic environment was obtained from electron microscopy data as described previously[13]. **(A)** Glutamate concentration time course at five distances from the release site. **(B)** The corresponding opening probability P_o of AMPA (upper panel) and NMDA (lower panel) receptors. The apparent extracellular diffusion coefficient for glutamate was set at 0.3 μm² ms⁻¹ (Ref. 28). Glutamate transporters were present at a concentration of 0.1 mM, which is equivalent to a surface density of ~10⁴ mol/μm² in glial membranes[10]. The resting extracellular glutamate concentration was set at 0.6 μM, which explains the tonic activation of NMDA receptors. Note that at distances comparable with the mean nearest-neighbour distance (NND; ~0.5 μm), the maximum P_o falls to a thirtieth of its original value for AMPA receptors but to only a quarter of its original value for NMDA receptors (the peak of the response at 0.5 μm was at >25 ms, which is outside the range of the x-axis).*

physiological data concerning properties of Ca^{2+} channels, in order to simulate extracellular Ca^{2+} transients, as explained in Box 3. Figure 4 shows the simulated time course of the extracellular Ca^{2+} level within and at different distances from the centre of the synaptic cleft. The results demonstrate that the action-potential-driven presynaptic Ca^{2+} influx that triggers exocytosis can deplete the level of the free ion in the cleft very rapidly (whereas outside the cleft Ca^{2+} levels remain almost unaffected). The level inside the cleft, however, returns to its resting value rapidly (within 1 ms) because of Ca^{2+} diffusion from the perisynaptic space. A more prolonged decrease in extracellular Ca^{2+} levels can occur following the opening of various postsynaptic Ca^{2+} channels. Their opening probability, and therefore the magnitude of the postsynaptic Ca^{2+} influx, depends on the membrane depolarization, which in turn depends on the synaptic activation of AMPA and NMDA receptors. Given that synaptic activation is likely to induce Ca^{2+} influx only through the spine-head membrane, changes in the extracellular Ca^{2+} concentration around neighbouring synapses are small (Fig. 4A). Only when the postsynaptic current is an order of magnitude larger than is thought to be a strong synaptic signal[33] does the Ca^{2+} depletion begin to affect neighbouring synapses, as illustrated in Fig. 4B. Although these data were computed for the resting extracellular Ca^{2+} concentration of 1 mM, other values for the resting levels produce similar profiles, provided that the Ca^{2+} influx is proportionately adjusted.

These data suggest that, unlike neurotransmitter spillover, the occurrence of synaptic crosstalk directly through the tissue volume, owing to extracellular Ca^{2+} depletion, is unlikely. An alternative mechanism, however, which could contribute to extracellular Ca^{2+} depletion, is the depolarization of the postsynaptic membrane that contains voltage-dependent Ca^{2+} channels[6,35]. Our previous simulation study explored a NEURON-built compartmental-cell model with dendritic spines that contained a mixed population of Ca^{2+} channels[36]. We used the time course of regenerative postsynaptic Ca^{2+} currents obtained in that study to drive Ca^{2+} influx in our present diffusion model. The results gave a profile of perisynaptic Ca^{2+} depletion, which was only 10–15 ms long but otherwise qualitatively similar to that in Fig. 4. In these simulations, dendritic 'spiking' and, therefore, significant Ca^{2+} depletion were observed when the peak conductance density of postsynaptic Ca^{2+} channels exceeded the range of ~10–20 pS/μm² (Ref. 36). This value is several times lower than the somatic membrane conductance (surface area of ~500–1000 μm²) predicted by the peak Ca^{2+} influx of 1–2 nA following an action potential generated at a giant axo–somatic synapse in the brainstem[37]. One factor that could, in principle, attenuate any long-term Ca^{2+} depletion, is the release of 'bound' Ca^{2+} ions that constitute the submembrane electrical double layer (see Box 3). However, it is less likely

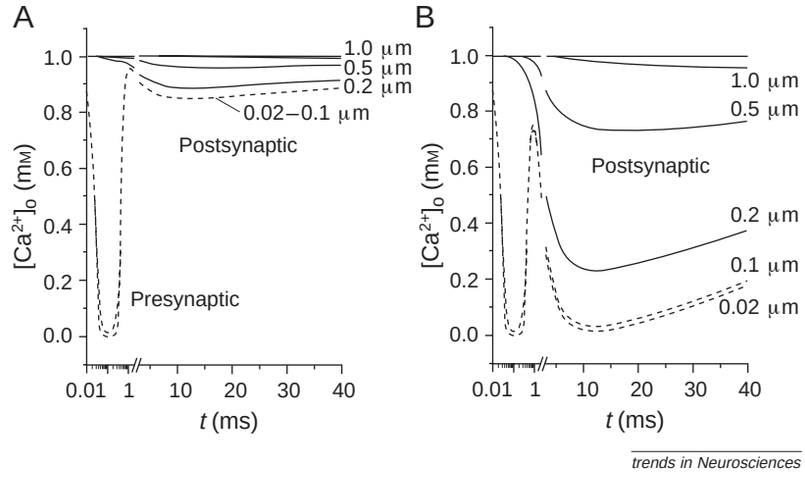

Fig. 4. ***Computed transients of extracellular Ca^{2+} concentration, $[Ca^{2+}]_o$, in the vicinity of axo–spinous synapses at five different distances from the release site.*** *The model uses the typical perisynaptic geometry assessed from electron microscopy as described previously[13]. The action potential drives fast Ca^{2+} influx through ten voltage-dependent Ca^{2+} channels (peak current, 0.5 pA) located at the presynaptic active zone that faces the synaptic cleft. The corresponding Ca^{2+} transient is indicated as presynaptic. The postsynaptic Ca^{2+} current is driven by NMDA-receptor-mediated depolarization[33], which is corrected for a 0.06 total current fraction through these receptors[34], and the corresponding Ca^{2+} transient is indicated as postsynaptic. **(A)** The condition of a strong synaptic input[33] with the postsynaptic Ca^{2+} current density i_{Ca}=5 pA/μm² equivalent to a peak current of ~1 pA through the dendritic spine membrane. **(B)** The condition of significant Ca^{2+} depletion that corresponds to i_{Ca}=40 pA/μm² (~8 pA through the spine membrane). Dotted and solid lines indicate the computed transients within the synaptic cleft and at different distances (shown) from the cleft centre, respectively.*

that this phenomenon has any effect on fast extracellular Ca^{2+} transients, and more experimental data are required to ascertain its spatial and temporal characteristics.

Concluding remarks

The mean inter-synaptic distance is an important constraint for physiological hypotheses that address crosstalk between synapses in the CNS. Building this constraint and other morphometric information into a realistic model of the synaptic environment reveals two mechanisms that could mediate inter-synaptic communication. First, NMDA-receptor-mediated crosstalk is likely to occur between conventional excitatory synapses in the hippocampus: the lower the apparent diffusion coefficient of glutamate, the more significant this phenomenon. This glutamate spillover phenomenon is likely to be especially important at the 30–50% of synapses that are separated by less than the mean NND (Refs 10,13,21) and could explain the observation that some synaptic release events are mediated exclusively by NMDA receptors[8]. Whether crosstalk occurs appreciably *in vivo* depends on the relatively poorly understood role of glutamate transporters. Transporters could either rapidly reduce the initial level of released neurotransmitter or, after one or two milliseconds, retard its diffusion, or both, in a temperature-dependent manner. Second, transient depletion of extracellular Ca^{2+} caused by the fast presynaptic influx that follows synaptic activation is unlikely to extend far beyond the synaptic cleft in CA1 (although it might do so at some calyceal synapses). Ca^{2+}-depletion-mediated crosstalk could potentially occur, however, if the elicited postsynaptic Ca^{2+} influx is five to ten times higher than can be produced by the estimated average individual synaptic signal that activates AMPA and NMDA receptors. Alternatively, the opening of extrasynaptic voltage-dependent Ca^{2+} channels in the postynaptic membrane could extend Ca^{2+} depletion to the extracellular space adjacent to the postsynaptic cell membrane outside the immediate synaptic cleft. How often the properties of individual synapses meet these crucial requirements for synaptic crosstalk remains to be ascertained experimentally. The conclusions of this study are related mainly to young adult animals, and additional data would be required to assess the plausibility of extrasynaptic communication in animals of different ages.

Acknowledgements
The authors thank Heather Davies and Elaine Harrison for help with electron-microscopy preparations, and Alan Fine and Leonid Savtchenko for their valuable comments. This work was supported by the Medical Research Council (UK) and Biotechnology and Biological Sciences Research Council (UK).

Selected References

1 **Isaacson, J.S. *et al.*** (1993) *Neuron* 10, 165–175
2 **Kullmann, D.M., Erdemli, G. and Asztely, F.** (1996) *Neuron* 17, 461–474
3 **Scanziani, M. *et al.*** (1997) *Nature* 385, 630–634
4 **Min, M.Y., Rusakov, D.A. and Kullmann, D.M.** (1998) *Neuron* 21, 561–570
5 **Montague, P.R.** (1996) *Proc. Natl. Acad. Sci. U. S. A. 93*, 3619–3623
6 **Egelman, D.M. and Montague, P.R.** (1998) *J. Neurosci.* 18, 8580–8589
7 **Barbour, B. and Häusser, M.** (1997) *Trends Neurosci.* 20, 377–384
8 **Kullmann, D.M. and Asztely, F.** (1998) *Trends Neurosci.* 21, 8–14
9 **Bergles, D.E. and Jahr, C.E.** (1997) *Neuron* 19, 1297–1308
10 **Lehre, K.P. and Danbolt, N.C.** (1998) *J. Neurosci.* 18, 8751–8757
11 **Borst, J.G.G. and Sakmann, B.** (1996) *Nature* 383, 431–434
12 **Helmchen, F., Borst, J.G.G. and Sakmann, B.** (1997) *Biophys. J.* 72, 1458–1471
13 **Rusakov, D.A. and Kullmann, D.M.** (1998) *J. Neurosci.* 18, 3158–3170
14 **Nicholson, C. and Rice, M.E.** (1987) *Can. J. Physiol. Pharmacol.* 65, 1086–1091
15 **Wall, M.J. and Usowicz, M.M.** (1997) *Eur. J. Neurosci.* 9, 533–548
16 **Rossi, D.J. and Hamann, M.** (1998) *Neuron* 20, 783–795
17 **Rusakov, D.A. *et al.*** (1997) *Neuroscience* 80, 69–77
18 **Brændgaar, H. and Gundersen, H.J.G.** (1986) *J. Neurosci. Meth.* 18, 39–78
19 **Geinisman, Y., DeToledo-Morrell, L. and Morrell, F.** (1986) *Proc. Natl. Acad. Sci. U. S. A.* 83, 3027–3031
20 **Rusakov, D.A., Harrison, E. and Stewart, M.G.** (1998) *Neuropharmacology* 37, 513–521
21 **Harris, K.M. and Ventura, R.** (1998) *Soc. Neurosci. Abstr.* 24, p. 827
22 **Barbour, B. *et al.*** (1994) *Neuron* 12, 1331–1343
23 **Nicholson, C.** (1995) *Biophys. J.* 68, 1699–1715
24 **Uteshev, V.V. and Pennefather, P.S.** (1997) *Biophys. J.* 72, 1127–1134
25 **Clements, J.D.** (1996) *Trends Neurosci.* 5, 163–170
26 **Clements, J.D. *et al.*** (1992) *Science* 258, 1498–1501
27 **Wahl, L.M., Pouzat, C. and Stratford, K.** (1996) *J. Neurophysiol.* 75, 597–608
28 **Rusakov, D.A. and Kullmann, D.M.** (1998) *Proc. Natl. Acad. Sci. U. S. A.* 95, 8975–8980
29 **Bergles, D.E. and Jahr, C.E.** (1998) *J. Neurosci.* 18, 7709–7716
30 **Asztely, F., Erdemli, G. and Kullmann, D.M. (1997)** *Neuron* 18, 281–293
31 **Nicholson, C. *et al.*** (1978) *J. Neurophysiol.* 41, 1026–1039
32 **Arens, J., Stabel J. and Heinemann, U.** (1992) *Can. J. Physiol. Pharmacol.* 70, S194–S205
33 **Zador, A. and Koch, C.** (1994) *J. Neurosci.* 14, 4705–4715
34 **Schneggenburger, R. *et al.*** (1993) *Neuron* 11, 133–143
35 **Stuart, G. *et al.*** (1997) *Trends Neurosci.* 20, 125–131
36 **Rusakov, D.A., Stewart, M.G. and Korogod, S.M.** (1996) *Neuroscience* 75, 315–323
37 **Bollmann, J.H. *et al.*** (1998) *J. Neurosci.* 18, 10409–10419

LETTERS TO THE EDITOR

On the role of NO in the thalamus

The article by Cudeiro and Rivadulla[1] is an important and timely review that attempts to provide an overview of the possible effects of NO in the visual system, and, as such, represents a novel way of interpreting the subject matter. In particular, the authors appear to suggest that in the lateral geniculate nucleus (LGN) of the thalamus, NO affects visual responses via a specific modulation of NMDA receptors that does not involve the guanylate cyclase–cGMP system. This interpretation rests to a significant extent on the finding made by Cudeiro and co-workers[2]: that iontophoretic application of 8-bromo-cGMP onto feline LGN neurones *in vivo* does not mimic the effects of NO donors.

We feel that in their endeavour the authors have not taken into consideration all of the available data concerning NO-related modulation of neurotransmission in the thalamus and, thus, provide an incomplete view of the function(s) of this modulator in the LGN and in other thalamic areas. There is now considerable *in vivo* physiological evidence to suggest that NO is released in the thalamus during arousal, most probably because of the activity of the cholinergic fibres ascending from the brainstem[3,4]. In addition, biochemical evidence suggests that these effects are mediated via cGMP (Refs 5,6). This suggestion is further supported by *in vitro* electrophysiological data[7], showing that NO donors cause a shift in the voltage dependence of the hyperpolarization-activated cation current I_h in thalamo–cortical neurones of the cat and guinea-pig lateral and medial geniculate nuclei, resulting in a membrane depolarization associated with a decrease in input resistance and interruption of rhythmic burst activity in these neurones. The effects of NO donors are occluded by cGMP analogues, indicating a common pathway of action. Taken together, these data suggest